

Controlled release of water-soluble astaxanthin from carboxymethyl cellulose/gelatin and octenyl succinic anhydride starch/gelatin blend films

Katarzyna Łupina^a, Dariusz Kowalczyk^{a,*}, Magdalena Lis^b, Aneta Raszewska-Kaczor^c, Emilia Drozłowska^d

^a Department of Biochemistry and Food Chemistry, Faculty of Food Sciences and Biotechnology, University of Life Sciences in Lublin, Skromna 8, 20-704, Lublin, Poland

^b Laboratory of Biocontrol, Application and Production of EPN, Faculty of Natural Sciences and Health, Center for Interdisciplinary Research, John Paul II Catholic University of Lublin, Konstantynów 1J, 20-708, Lublin, Poland

^c Łukasiewicz Research Network - Institute for Engineering of Polymer Materials and Dyes, Marii Skłodowskiej-Curie 55, 87-100, Toruń, Poland

^d Center of Bioimmobilisation and Innovative Packaging Materials, Faculty of Food Sciences and Fisheries, West Pomeranian University of Technology, Klemensa Janickiego 35, 71-270, Szczecin, Poland

ARTICLE INFO

Keywords:

Polysaccharides
Edible films
Astaxanthin
Release kinetics
Antioxidant activity

ABSTRACT

The effect of increasing concentrations (0, 0.25, 0.5, 1%) of commercial water-soluble AstaSana astaxanthin (AST) on the physicochemical properties, release kinetics and antioxidant activity of binary 75/25 carboxymethyl cellulose/gelatin (CMC75/GEL25) and octenyl succinic anhydride starch/gelatin (OSA75/GEL25) blend films was investigated. The microscopic observations showed that the obtained blends were phase-separated systems. Regardless of the AST concentration, the CMC-based films were more opaque, stronger, and less stretchable than the OSA-based films. The AST-supplemented films exhibited an intensive red color. The starch granules (from the AST formulation) contributed to high roughness and opacity of the films. The presence of AST contributed to a significant decrease of the puncture strength and oxygen permeability of the CMC-based film. The AST-supplemented films did not differ in terms of the water vapour barrier properties. Due to the low quantity of astaxanthin in the systems, the Fourier-transform infrared spectra of the control and AST-supplemented films were similar. The increase in the AST concentration was accompanied by reduced solubility and increased swelling of the OSA-based films, while an opposite result was observed for the CMC-based films. According to the Korsmeyer-Peppas with time lag model, the AST release kinetics exhibited quasi-Fickian behaviour. Due to their weaker solubility, the OSA75/GEL25 films offered at least 7 times slower release of AST than the CMC-based carrier. The times required for 25% AST release from the CMC75/GEL25 and OSA75/GEL25 films were 1.20–1.74 and 12.60–20.04 min, respectively. A high positive correlation ($R^2 = 0.78–0.91$) was found between the AST release and antiradical activity of the films.

1. Introduction

The dynamic development of the packaging market is closely related to the necessity of extension of the shelf life of food products in response to the demands of both producers and consumers. Hence, efforts are being made to expand the functions of traditional packaging, e.g. through fortification thereof with food preservatives whose action and/or release from the packaging take place in a controlled manner.

The depletion of crude oil resources generates increasing pressure from environmentalists aimed at the replacement of plastic packaging with materials made of natural biodegradable polymers. Cellulose and

starch are abundant and cheap biopolymers that can serve as more eco-friendly alternatives to synthetic polymers. Both these polymers have numerous derivatives with modified functionalities, which can be used to produce packaging materials with desired properties. Films produced from cellulose derivatives (e.g. carboxymethyl cellulose (CMC), methylcellulose, or hydroxypropyl methylcellulose) are highly transparent, mechanically strong, and easily soluble in water (Bourtoom, 2008). In turn, hydrophobised starch, such as octenyl succinic anhydride starch (OSA), is an effective film-forming emulsifier and encapsulation agent for active substances (Aćkar et al., 2015; Łupina, Kowalczyk, & Drozłowska, 2020).

* Corresponding author.

E-mail address: dariusz.kowalczyk@up.lublin.pl (D. Kowalczyk).

<https://doi.org/10.1016/j.foodhyd.2021.107179>

Received 2 March 2021; Received in revised form 2 August 2021; Accepted 5 September 2021

Available online 7 September 2021

0268-005X/© 2021 The Author(s). Published by Elsevier Ltd. This is an open access article under the CC BY license (<http://creativecommons.org/licenses/by/4.0/>).

Polymer blend composites are versatile materials offering synergism in properties for a wide array of phenomenal applications, including packaging and controlled release purposes. Previous studies (Kowalczyk, Kordowska-Wiater, et al., 2020; Kowalczyk, Pytko, et al., 2020; Lupina et al., 2020) have shown that a combination of some polysaccharides and gelatin (GEL) yields materials with improved properties and modified profiles of active compound release. For instance, the CMC/GEL films offered the quick release of active substances ('burst effect') (Kowalczyk, Pytko, et al., 2020). In turn, the OSA/GEL blend system ensured the encapsulation of active compounds through the formation of complex coacervates (Zhao et al., 2019).

Since food products contain many oxidation-susceptible substances, packaging materials with incorporated antioxidants arouse great interest. Carotenoids are pigments that perform a variety of critical functions in plants including the protection against photooxidative processes (Stahl & Sies, 2003). For industry needs, carotenoids are obtained by chemical synthesis or extraction from plants or algae. Natural carotenoids exhibit low stability, variable dye composition (it is not easy to standardize their color), the specific taste and smell, and auxiliaries. These disadvantages can be avoided by the use of synthetic dyes, which exhibit significantly higher resistance and dye strength. In addition, chemical synthesis does not require a large amount of raw material. Of the nearly 700 naturally occurring carotenoids, only a few (lycopene, canthaxanthin, astaxanthin (ASX), β,β -carotene, β -apo-8'-carotene, β -apo-8'-carotene, and cytranaxanthin) are synthesized on an industrial scale (Bogacz-Radomska & Harasym, 2018). Among them especially ASX is gaining enormous popularity because of reports on its multidirectional biological activity, in particular the high antioxidant effect, which (in the case of natural ASX) can be up to 100 times greater than that of α -tocopherol (Ambati, Moi, Ravi, & Aswathanarayana, 2014).

ASX (3,3'-dihydroxy- β,β' -carotene-4,4'-dione) comprises a non-polar polyene carbon chain terminated on both sides by β -ionone rings. The structure of the pigment is very similar to that of other carotenoids; however, the presence of hydroxyl and ketone groups in each ring is responsible for its partially hydrophilic nature. Its polar ends provide the molecule with esterification capacity, an affinity for phospholipids, and higher antioxidant activity. The specific polar-non-polar structure of ASX is analogous to the structure of the cell membrane, which facilitates the removal of reactive oxygen species and free radicals both on the outer and inner membrane surface (Santos-Sánchez, Hernández-Carlos, Torres-Ariño, & Salas-Coronado, 2020). The ASX molecule has two asymmetric carbon atoms in positions 3,3' of the β -ionone ring; hence, the pigment can exist as two enantiomers (3R, 3'R, and 3S, 3'S) and a meso compound (3R, 3'S) (Ye, Fan, Keen, & Han, 2019). The thirteen conjugated double bonds present in the ASX molecule are responsible for its red colour and, to some extent, for its antioxidant activity (Higuera-Ciajara, Félix-Valenzuela, & Goycoolea, 2006; Santos-Sánchez et al., 2020).

Microalgae (mainly *Haematococcus pluvialis*) is expected to be one of the largest and fastest-growing natural sources of ASX. These organisms are at the base of the food web of marine species; hence, the pigment is eventually accumulated in tissues of various fish species (salmon, trout, red bream) and crustaceans (shrimp, lobster). Natural ASX is highly susceptible to degradation during processing and storage, i.e. it is decomposed upon contact with oxygen, light, low pH, some enzymes, or certain food ingredients (Liu, Zhang, McClements, Wang, & Xu, 2019). ASX degradation has been reported to be reduced by the addition of other antioxidants (Martínez-Delgado, Khandual, & Villanueva-Rodríguez, 2017). Meléndez Martínez, Vicario Romero, and Heredia Mira (2004) have found that carotenoids are better preserved in tocopherol- and vitamin C-containing foods; hence, the presence of these antioxidants in ASX-rich formulations seems to be advisable. A complementary form of ASX protection against degradation is microencapsulation (e.g. in the chitosan matrix, OSA/GEL coacervates, polymer-based nanospheres, emulsions, and liposomes) or formation of complexes with β -cyclodextrins.

Despite the possibilities of enhancing the stability of the natural ASX, the most serious obstacle preventing its industrial-scale application is associated with its high production costs. The market value of natural ASX varies usually from \$2500–7000/kg, while synthetically derived ASX costs around \$1000/kg (Panis & Carreon, 2016). Additionally, the natural ASX is very poorly soluble in water, which also considerably limits its application. Natural and synthetic ASX is not exactly the same, as they differ in the esterification degree and stereochemistry. Currently, two forms of synthetic ASX can be produced: disodium disuccinate ASX (DDA) and Cardax's proprietary ASX prodrug (CDX-085). DDA is a mixture of three isomers. This form is used in studies on cardiovascular system diseases. It can be served by the oral or intravenous route and its advantage is good water solubility. The CDX-085 ASX has better dispersion in water and greater bioavailability than the DDA. The modified structure makes synthetic ASX much more convenient for commercial use. However, a significant drawback of chemically produced ASX is its lower antioxidant activity, in comparison with that of the natural pigment. It also raises controversial issues related to the production technique thereof (Capelli, Bagchi, & Cysewski, 2013). Nevertheless, it is estimated that the synthetic compound accounts for approximately 95% of ASX contained in various types of formulations available on the global market (Panis & Carreon, 2016; Shah, Liang, Cheng, & Daroch, 2016; Sieradzka & Kołodziejczyk-Czepas, 2016). ASX is available in the form of biomass, oils, extracts, powders, capsules, gels, and tablets (Ambati et al., 2014).

Both natural and synthetic ASX has been assessed for safety and found safe for human consumption in a number of jurisdictions and in various regulatory categories (Brendler & Williamson, 2019). European Food Safety Authority (EFSA) estimated the acceptable daily intake of natural ASX at 0.034 mg/kg body weight, i.e. approximately 2 mg per day for an adult with a bodyweight of 60 kg (an analogous dose was established for synthetic ASX) (EFSA, 2014).

So far, limited studies were conducted on the fabrication of ASX-added packaging materials. Colín-Chávez, Soto-Valdez, Peralta, Lizardi-Mendoza, and Baladrán-Quintana (2013b) incorporated Aztec marigold (*Tagetes erecta*) extract (source of ASX) into the polyethylene active packaging films in order to assess the ASX migration into a fatty food stimulant (95% ethanol) at different temperatures (10, 23, 30, and 40 °C). As expected, the increase in temperature resulted in higher ASX diffusion coefficients. In another study, Gómez-Estaca, Calvo, Sánchez-Faure, Montero, and Gómez-Guillén (2015) obtained the shrimp muscle protein film incorporated with an oil extract of shrimp wastes (source of ASX). The active film exhibited a faster release of carotenoids and, consequently, higher antioxidant activity as compared to the films containing tomato extract (source of lycopene) or β -carotene. Furthermore, ASX showed the slowest degradation during storage. The addition of the extract caused a significant improvement of water vapour barrier properties of the film, but at the same time worsening the opacity, which was due to the presence of the emulsified lipid phase in the film matrix.

In this study, synthetic ASX was used not only to reduce the costs of active film production but also to avoid incorporation of the solvent (oil) into biopolymer carriers, which could prevent the formation of coherent films or yielded emulsion materials with reduced functional properties. Therefore, a commercial AstaSana™ 5% CWS/S-TG (AST) formulation containing water-soluble ASX was used in the experiments. The main objective of this study was to characterise the physicochemical, release and antioxidant properties of binary 75/25 carboxymethyl cellulose/gelatin (CMC75/GEL25) and 75/25 octenyl succinic anhydride starch/gelatin (OSA75/GEL25) blend films supplemented with increasing concentrations (0, 0.25, 0.5, 1%) of AST. The release properties are discussed in terms of the microstructure and water affinities (dissolution and swelling) of the films.

2. Materials and methods

2.1. Materials

The following commercial food-grade biopolymers were used in this study: sodium CMC WALOCEL CRT 30 GA (with substitution degree of 0.82–0.95; Dow Wolff Cellulosics, Germany), starch sodium octenyl succinate Purity Gum® 2000 (Ingredion, Germany), and pork GEL (with bloom strength of 240; McCormick-Kamis S.A., Poland). AstaSana™ 5% CWS/S-TG (containing astaxanthin, modified food starch, corn starch, glucose syrup, sodium ascorbate, and DL- α -tocopherol) was gifted by DSM Nutritional Products (Netherlands). Glycerol and 2,2'-azino-bis(3-ethylbenzothiazoline-6-sulfonic acid) diammonium salt (ABTS) were purchased from Sigma Chemical Co. (USA).

2.2. Film preparation

Films were obtained from aqueous solutions containing the polysaccharide/GEL blend (5% w/w), glycerol (1% w/w), and increasing amounts of AST (0.25, 0.5, 1% w/w). The film-forming solution (FFS) without added AST served as the control. Powder blends of polysaccharides with GEL at the ratio of 75/25 were mixed with water and glycerol and then heated in a water bath at 90 °C for 1 h with constant stirring. The FFSs were allowed to cool (to ~40 °C) and the AST was subsequently added (Fig. 1). The degassed FFSs were placed on the

polycarbonate trays with an area of 144 and 4 cm². A constant amount of total solids (0.0125g/cm²) was placed on the trays in order to maintain film thickness. The FFSs were dried at 25 ± 2 °C and 50 ± 5% relative humidity (RH) for 24 h. The films were peeled from the trays, cut into sample pieces, and conditioned.

2.3. pH

A glass electrode (Elmetron ERH-11S, Poland) connected to a pH meter (Elmetron CPC 401, Poland) was used for measurement of pH of the FFSs at 40 °C. The tests were performed in triplicate.

2.4. Film thickness and conditioning

The thickness of the film samples was determined using a 547-401 ABSOLUTE digimatic thickness gauge (Mitotuyo, Japan). The samples were conditioned (50% RH, 25 °C, 48 h) in a test chamber (MLR-350, Sanyo Electric Biomedical Co. Ltd., Japan).

2.5. Microscopy

The morphology of the FFSs was examined using an inverted microscope (CKX53, Olympus, Japan) at 40 °C as well as a Carl Zeiss Ultra Plus scanning electron microscope (Oberkochen, Germany) using a cryo-scanning electron microscopy (cryo-SEM). Additionally, the 1% aqueous

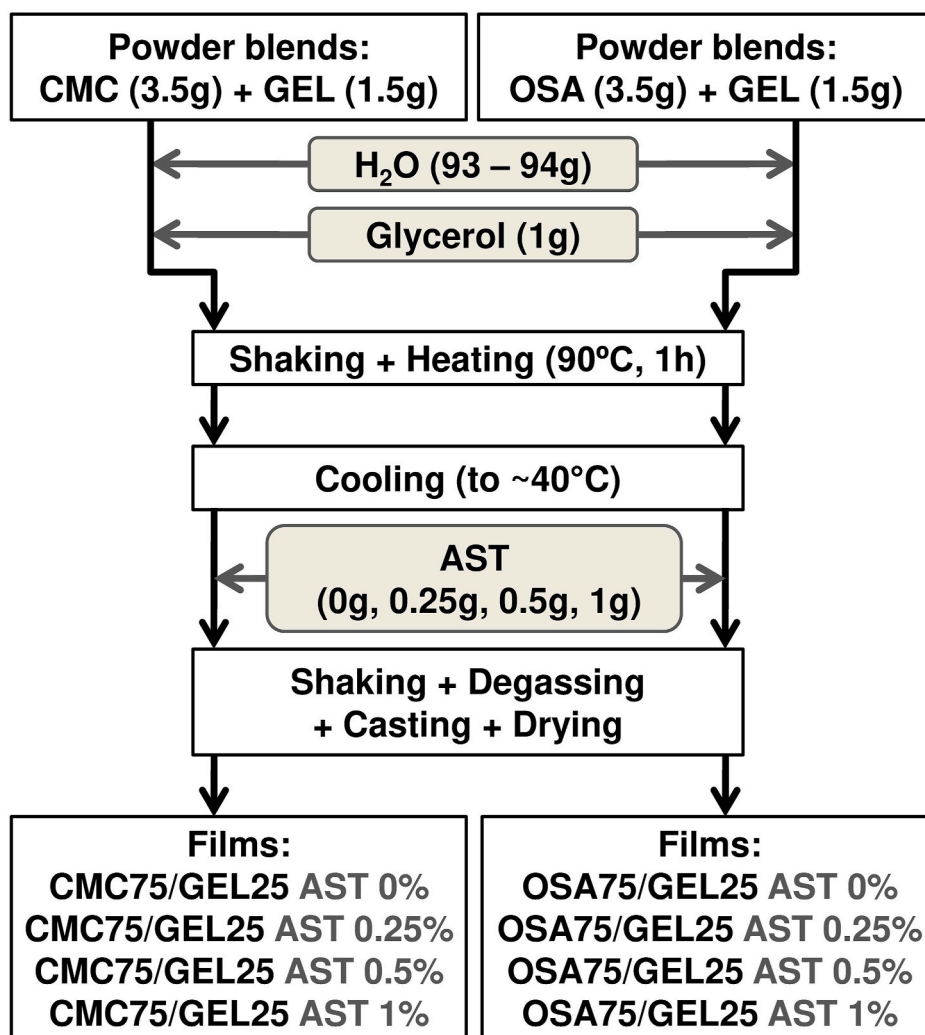


Fig. 1. Schematic diagram showing the procedure for obtaining the 75/25 carboxymethyl cellulose/gelatin (CMC75/GEL25) and 75/25 octenyl succinic anhydride starch/gelatin (OSA75/GEL25) blend films.

solution of AST was observed using these microscopes and a polarised light microscope LEICA 5500B (Leica Microsystems GmbH, Germany). Moreover, SEM was used for inspection of the surface of the AST powder.

2.6. Attenuated Total Reflection Fourier Transform Infrared (ATR-FTIR) Spectroscopy

ATR-FTIR tests were carried out by using a Thermo Nicolet 8700 FTIR spectrometer with a Smart Orbit accessory.

2.7. Color and opacity

Lightness (L^*), chroma (C^*), and hue angle (h) of the film samples (1×4 cm) were measured with a colorimeter (NH310, 3nh, China) on the white background ($L^* = 93.84$, $C^* = 10.42$, $h = 271.96^\circ$). The opacity (Op) of the film samples (1×4 cm) was measured at 600 nm using a spectrophotometer (Lambda 40, Perkin-Elmer, USA), and calculated with the following formula (Han & Floros, 1997):

$$Op = A_{600} / x \quad (1)$$

where A_{600} is the absorbance at 600 nm and x is the film thickness (mm).

The optical analyses were performed in fivefold.

2.8. Mechanical properties

The mechanical properties of films were evaluated using a TA-XT2i texture analyzer equipped with a 50 kg load cell (Stable Micro Systems, UK). A steel ball-ended (2 mm diameter) probe was moved perpendicularly at the film surface at a constant speed (1 mm s^{-1}) until it passed through the film. The puncture strength (PS, MPa) was calculated by Eq. (2):

$$PS = F/A \quad (2)$$

where F is the maximum force (N) and A is the cross-sectional area of the probe (films thickness \times diameter of the opening of film holder, mm^2).

A puncture deformation (PD, mm) was read at the sample breaking point.

2.9. Contact angle (CA)

The water wetting properties of the samples were measured using a goniometer (Phoenix Mini, Surface Electro Optics, Korea). A droplet of distilled water was deposited on the film surface. The CA measurements were carried out on the "air-side" of the films. The measurements were performed at least three times at random positions on samples.

2.10. Swelling (Sw) and total soluble matter (TSM)

Sw was evaluated by immersing the pre-weighed films (4 cm^2) into 25 ml of distilled water at $30 \pm 1^\circ \text{C}$ for 1 min. The weight of the swollen films was measured after blotting the surface gently with filter paper until equilibrium was reached. Sw was calculated as the percentage of water absorbed by the sample. TSM was expressed as the percentage of film dry matter solubilised after immersion in water. The film specimens (4 cm^2) were weighed ($\pm 0.0001 \text{ g}$) and shaken (Shaking Incubator ES-60, MIULAB, China) in 25 ml of distilled water at $30 \pm 1^\circ \text{C}$ and 170 rpm. Then, undissolved residues taken at 10 different time points were removed from the water and dried (105°C , 24 h). The initial dry matter content of the films, necessary for the calculation of TSM, was determined by drying at 105°C for 24 h. The tests were performed in triplicate.

2.11. Water vapour permeability (WVP)

The WVP ($\text{g mmm}^{-2} \text{d}^{-1} \text{kPa}^{-1}$) was calculated as:

$$WVP = (WVTR \times L) / \Delta p \quad (3)$$

where WVTR is the water vapour transmission rate of film ($\text{g m}^{-2} \text{d}^{-1}$) measured gravimetrically based on ISO 2528 (1995) method, L is the mean of film thickness (mm), Δp is the water vapour pressure difference (kPa) between two sides of the film.

The permeation cell (poly(methyl methacrylate)) cups had an internal diameter of 7.98 cm (exposed film area = 50 cm^2) and an internal depth of 2 cm. Distilled water (30 ml) was added into each test cup and film samples were placed over the circular opening and secured by a screw top. The cups were placed in the test chamber set at 25°C and 50% RH. The weight loss from the samples with 3 replicates was monitored for 10 h period with weights recorded at 2 h intervals.

2.12. Oxygen transmission rate (OTR)

OTR was measured using a MultiPermeO₂-CO₂ (Extra Solution Instrument, Italy) instrument. Permeability measurements through film area (50 cm^2) were conducted at 23°C and RH $50 \pm 3\%$. The test gas was oxygen (purity $\geq 99.95\%$), while the carrier gas was a nitrogen (5.0) containing 1% of hydrogen. The tests were done by obtaining a steady line for transmission rate. Three samples were tested for each type of material and average results of OTR (expressed as the volume of permeant passing through a film, per unit area and time, normalized on the thickness ($\text{cm}^3 \mu\text{m}/(\text{m}^2 \text{d})$) are presented.

2.13. Release test

The film discs (4 cm^2) were immersed in 25 ml of distilled water at $30 \pm 1^\circ \text{C}$ and shaken (170 rpm; $30 \pm 1^\circ \text{C}$) in a shaking incubator. Samples of the release media (250 μl) were taken at different time points, and the absorbance was read at 464 nm using a microplate spectrophotometer (EPOCH 2 Microplate Spectrophotometer, BioTek, USA). The tests were performed in triplicate. The AST release kinetics was modeled using DDSolver: add-in software for Microsoft Excel. Several mathematical models were chosen to fit the data (Table S1). The adjusted coefficient of determination (R^2_{adjusted}) was used for the selection of the optimal model. On the basis of the best-fitted model, the quarter- and half-release time values ($t_{25\%}$ and $t_{50\%}$) were calculated (Zhang et al., 2010).

2.14. ABTS free radical scavenging ability

The film discs (4 cm^2) were immersed in 25 ml of the ABTS reagent at 30°C and mixed using a laboratory shaker (170 rpm). The mixture samples (250 μl) were taken at different time points, and the absorbance was read at 734 nm using a spectrophotometer (Lambda 40, Perkin-Elmer, Shelton, CT, USA) in order to determine the degree of scavenging of ABTS free radicals. The absorbance was measured until the reaction reached a plateau. The ability of the films to quench ABTS free radicals was calculated using Eq. (4).

$$\text{Scavenging\%} = [1 - (\text{Abs}/\text{Abs}_{\text{ABTS}})] \times 100 \quad (4)$$

where Abs is the absorbance of the sample and Abs_{ABTS} is the absorbance of the ABTS solution (0.70 ± 0.05). The tests were performed in triplicate.

2.15. Statistical analysis

Differences among the mean values of the data were tested for statistical significance at the $p < 0.05$ level using analysis of variance (STATISTICA 13.1, StatSoft Inc., Tulsa, USA) and Fisher's test.

Additionally, the data were evaluated using Pearson's correlation coefficients to identify relationships between the TSM, the AST release, and the ABTS free radical scavenging ability.

3. Results and discussion

3.1. Microstructure

The micrographs (prepared both using a cryo-SEM technique and an optical microscope) of the CMC75/GEL25 FFSs revealed the presence of spherical structures with various diameters (11–68 μm , Fig. 2A and B). As demonstrated in a previous study (Kowalczyk, Pytka, et al., 2020), the microspheres (rich in GEL) are indicator of the phase separation between the polymers. The OSA-based FFSs had a sandy structure (Fig. 2B), which supports our earlier findings (Lupina et al., 2020). The observed inhomogeneity of this system may be explained by the fact that anionic OSA and cationic GEL form complex coacervates through electrostatic interactions (Wu & McClements, 2015; Zhao et al., 2019). Fig. 2C–a shows that AST consists of free-flowing particles. The round objects with different sizes (8–48 μm) were found both in the AST-supplemented FFSs (Fig. 2B) and the aqueous AST solution (Fig. 2C–b). Since starch is the carrier in the AST formulation, it is easy to conclude that the observed particles were starch granules. The observation of the AST solution under a polarised optical microscope revealed the presence of Maltese crosses, which are characteristic of starch granules (Fig. 2C–c). It is worth mentioning here that it was hard to detect the starch granules in the samples using the SEM technique (Fig. 2A; Fig. 2C–a; Fig. 2C–d). which may be explained by the fact that only a small part of the samples was analysed at higher magnifications.

3.2. ATR-FTIR Spectroscopy

Fig. 3 shows the ATR-FTIR spectra of the control and 1%AST-supplemented films. Strong broadband at 3272–3287 cm^{-1} resulting from amide A (-OH and/or -NH₂) stretching can be seen in the spectra of all samples. The absorption peaks at ~ 2930 and ~ 2880 cm^{-1} (in the Amide B band) are related to CH₂ asymmetrical and CH₂ symmetrical stretching (Lupina et al., 2019). The peak in the 1633–1646 cm^{-1} region originates from C=O stretching vibration in the Amide 1 band (Kowalczyk, Pytka, et al., 2020). According to the previous study (Lupina et al., 2019), the peak at 1630–1695 cm^{-1} is characteristic for the -CONH₂ group and its occurrence suggests that the polysaccharides and GEL were strongly associated in the blend films. The peaks centered at 1589, 1410, and 1321 cm^{-1} are attributed to the COO⁻ (carboxyl) group in the CMC (Kowalczyk, Pytka, et al., 2020). In the case of the OSA-based films, the asymmetric stretching vibration of carboxylate appeared at 1555 cm^{-1} . The signal at 1148 cm^{-1} in the spectrum of the OSA75/GEL25 film is related to C–O stretching present both in the structure of starch (Hejna, Lenza, Formela, & Korol, 2019) and in GEL (Jafari, Emami, Samadikuchaksaraei, Bahar, & Gorjipour, 2011). The spectra of all films showed a strong absorption band at ~ 1020 cm^{-1} indicating the presence of the C–N group (Coates, 2006). The locations of peaks in the spectra of the 1%AST-supplemented films were similar to those of the control (Fig. 3), which could be explained by the relatively low quantity of AST in the systems. These results support evidence from previous observations (Yuan, Jin, & Xu, 2012). Generally, no new peaks occurred in the spectra. Nevertheless, it was found that the presence of AST in the film matrix slightly increased the intensity of peaks located at 1647–1100 cm^{-1} , which may have resulted from some AST/polymer interactions. To date, limited data are available on the possible interactions of the water-soluble (synthetic) ASX with biopolymers. Nevertheless, the specific interactions between natural ASX and CMC as well as proteins (bovine serum albumin) have been previously suggested (Feng, Li, Wang, & Zhu, 2018; Y.; Liu et al., 2020).

3.3. Optical properties

The AST-free CMC- and OSA-based films were colourless to the naked eye (Fig. S1) and had similar L*C*h coordinates, according to which were bright ($L^* \approx 94$) with a blue shade ($h \approx 270^\circ$) of very low saturation ($C^* \approx 9$) (Table 1). Likely due to the presence of phase-separated microspheres (Fig. 2A and B), the CMC75/GEL25 films exhibited higher Op than the OSA-based counterparts ($p < 0.05$, Table 1). The incorporation of AST resulted in the red-colour and less transparent films (Fig. S1, Table 1). AST decreased the L*C*h parameters in a concentration-dependent manner (Table 1); i.e. the color of the films became darker, less deep (more neutral), and more shifted toward red hue ($h = 0^\circ$). Furthermore, with an increase in the AST concentration, the gradual decrease in film transparency was observed (Table 1), which could be primarily explained by the increasing number of starch granules (from the AST formulation (Fig. 2B)), that could reflect or scatter a significant amount of light. Surprisingly, the 0.25%AST-added films exhibited the most intense colour saturation (the highest C* values, Table 1). This result can be attributed to the fact that among all AST-supplemented films, these films were the most transparent and, consequently, the lightest (Table 1). Because of higher ASX content, the films obtained in our study (the amount of pure ASX added was 0.0025–0.01 g/g polymer fraction) were nearly two times darker and approximately two to four times more red (based on L* and h values) as compared to the shrimp protein-based film enriched with shrimp extract (0.001g ASX/g protein) (Gómez-Estaca et al., 2015).

3.4. Mechanical properties

According to the PS test, the CMC-based films were ~ 4 –5 times stronger than the OSA-based counterparts (8.75–11.80 vs 1.96–2.32 MPa, Table 2). The possible causes for this behavior have been suggested previously (Kowalczyk & Baraniak, 2014; Lupina et al., 2019). Briefly, the linear backbone of cellulose results in more extensive hydrogen intermolecular bonds than in starch, which is a mixture of branched amylopectin and linear amylose. Branches make it difficult for the amylopectin molecules to pack in a regular array and therefore make the starchy network less tough. The presence of AST did not affect the PS of OSA-based films, whereas contributed to a significant decrease of the mechanical strength of the CMC-based film (Table 2). This result supports evidence from previous observations (Kowalczyk & Biendl, 2016), which showed that the less organized network of oxidised potato starch-based film was not susceptible to mechanical changes in the presence of hop phytoconstituents, while the more cohesive network of the CMC-based film was weakened, likely due to interruption of hydrogen bonding networks of the polysaccharide by the active compounds.

The OSA-based films were at least two times more deformable compared to the CMC-containing films (Table 2). This result reflects earlier studies (Kowalczyk et al., 2021; Lupina et al., 2019), which showed that OSA/GEL blends form several times more stretchable films than the methylcellulose/GEL or CMC/GEL blends. It was found that at the smallest addition level (0.25%), AST significantly increased the elasticity of the CMC75/GEL25 film (Table 2). It shows that when incorporated into the CMC/GEL blend system at low concentration, AST can increase the free volume between the polymer segments which allows for increased movement of chain chains with respect to each other, consequently, increasing the film ability for being stretched.

3.5. pH, CA, Sw, and TSM

The FFSs based on CMC (more exactly: the sodium salt of CMC) exhibited higher pH values than the FFSs based on OSA (more exactly: starch sodium octenyl succinate) (6.10–6.35 vs. 4.80–4.89, Table 2). This finding was unexpected since both polysaccharides contain an alkali metal in the structure. However, the higher acidity of OSA-based

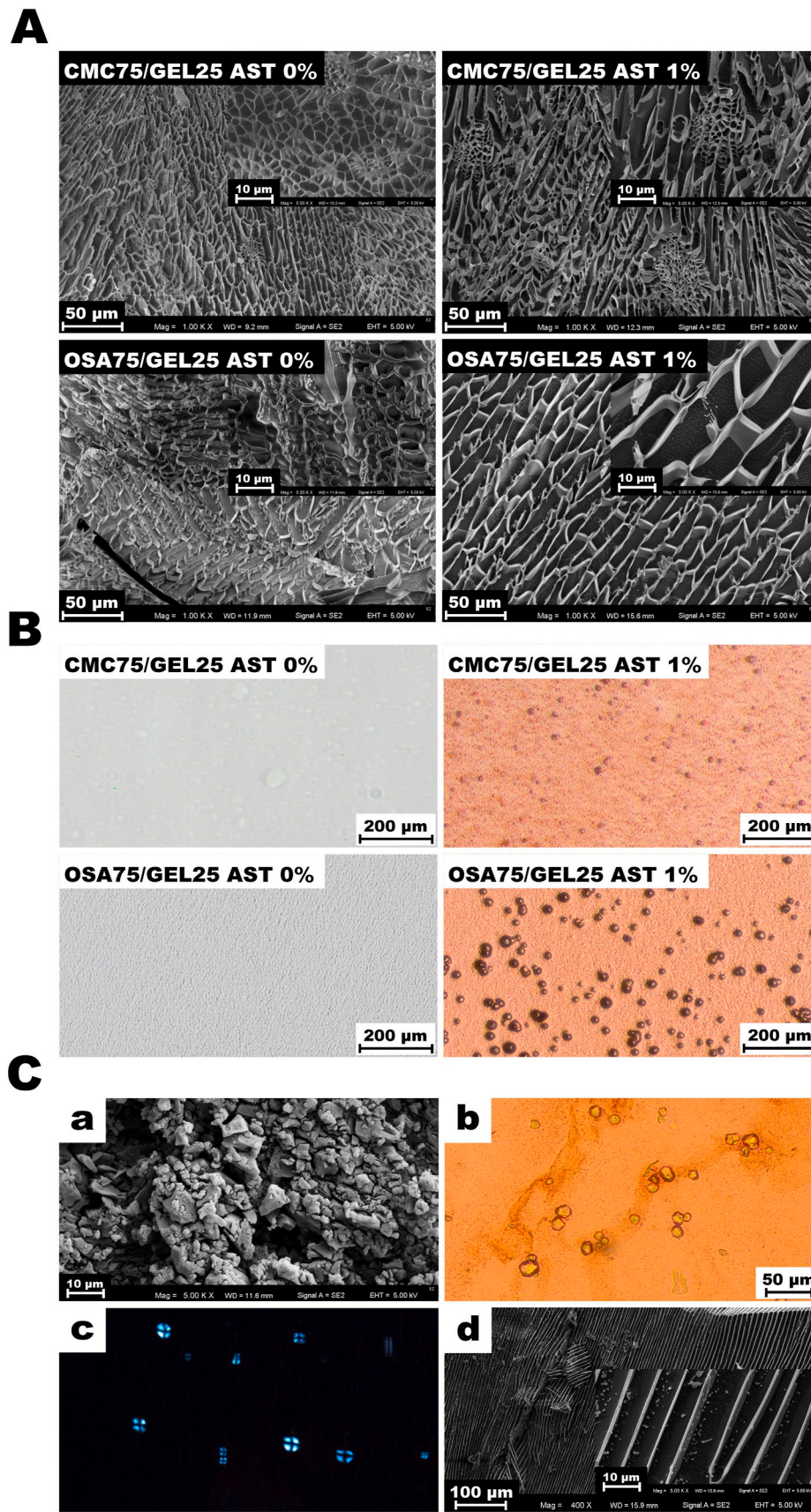


Fig. 2. Images of 75/25 carboxymethyl cellulose/gelatin (CMC75/GEL25) and 75/25 octenyl succinic anhydride starch/gelatin (OSA75/GEL25) film-forming solutions with and without Astasana (AST) addition examined using the cryo-SEM technique (A) and the light microscope (B). Microstructure of AST powder (C-a). Images of the 1% (w/v) aqueous solution of AST taken with the light microscope (C-b), the polarising microscope (C-c), and the cryo-SEM technique (C-d).

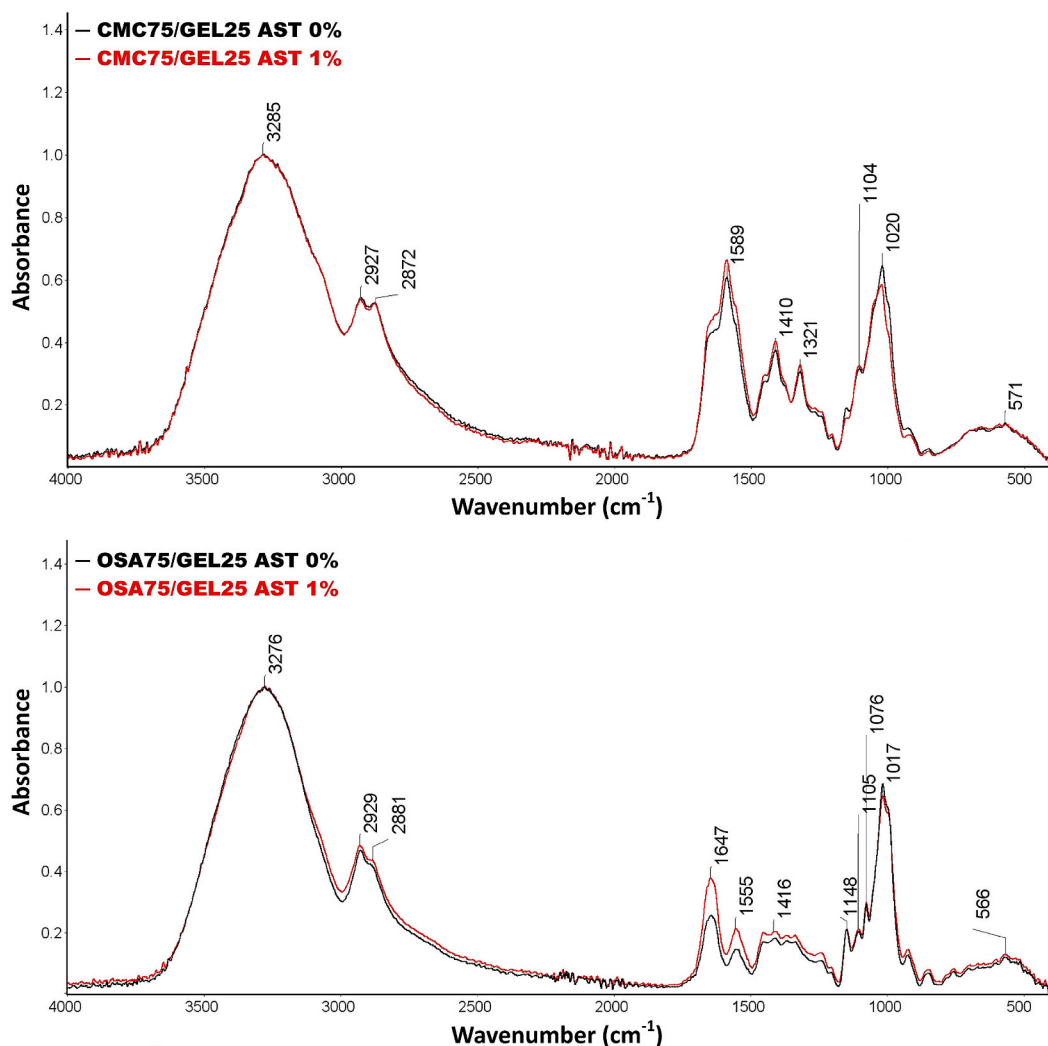


Fig. 3. Attenuated Total Reflection Fourier Transform Infrared spectra of the 75/25 carboxymethyl cellulose/gelatin (CMC75/GEL25) and 75/25 octenyl succinic anhydride starch/gelatin (OSA75/GEL25) blend films with and without Astasana (AST) addition.

Table 1

The effect of Astasana (AST) concentration on the color parameters (L^*C^*h) and opacity (Op) of the 75/25 carboxymethyl cellulose/gelatin (CMC75/GEL25) and 75/25 octenyl succinic anhydride starch/gelatin (OSA75/GEL25) films.

Film	AST (%)	L^*	C^*	h	Op (A_{600}/mm)
CMC75/ GEL25	0	93.74 ± 0.11 ^f	8.21 ± 0.08 ^a	270.17 ± 0.65 ^f	1.38 ± 0.06 ^b
	0.25	44.01 ± 0.46 ^c	55.64 ± 0.28 ^h	27.56 ± 0.40 ^e	5.82 ± 0.42 ^d
	0.5	38.80 ± 0.57 ^c	47.83 ± 0.75 ^f	21.44 ± 0.98 ^e	9.62 ± 0.69 ^f
	1	33.79 ± 0.33 ^a	35.37 ± 1.04 ^d	15.00 ± 0.40 ^a	16.74 ± 0.77 ^h
OSA75/ GEL25	0	94.15 ± 0.20 ^f	9.69 ± 0.20 ^b	272.61 ± 0.72 ^e	0.61 ± 0.05 ^a
	0.25	43.14 ± 0.63 ^d	54.63 ± 0.77 ^g	25.54 ± 0.68 ^d	4.42 ± 0.36 ^c
	0.5	38.06 ± 0.12 ^b	44.16 ± 0.32 ^c	18.87 ± 0.14 ^b	8.12 ± 0.20 ^e
	1	34.09 ± 0.37 ^a	32.40 ± 0.57 ^c	14.47 ± 0.40 ^a	14.54 ± 0.16 ^g

^{a-h} Values with the different superscript letters within one column are significantly different ($p < 0.05$).

FFSs could be explained by the presence of acid anhydride residues. In the case of all FFSs, the pH value was reduced after the incorporation of AST.

The wetting properties of the solid surface can be identified by analysis of the value of the CA. Materials with CAs $< 90^\circ$ are defined as hydrophilic; in turn, the CAs $> 90^\circ$ reflect the hydrophobic properties. It was found that the control films did not differ in terms of wetting properties (Table 2). In the case of CMC-based film the addition of AST at the level of 0.25–0.5% decreased the CA; i.e. made the surface more wettable. In turn, in the case of OSA-based film, the incorporation of AST at the level of 1% increased the surface hydrophobicity.

Since the obtained films were water-soluble (Fig. 4), their Sw values were determined only for the first 1-min contact with water. The control CMC film exhibited significantly higher Sw (831.60%) than the OSA/GEL blend films are highly hydrophilic and can absorb substantial amounts of water before they start to dissolve (Kowalczyk, Pytka, et al., 2020). The low Sw of the OSA-based films could be partially attributed to the presence of hydrophobic octenyl side chains in the polysaccharide (Tesch, Gerhards, & Schubert, 2002), which limited the permeation of water into the polymeric matrix. In the case of the CMC75/GEL25 carrier, the incorporation of AST yielded films with reduced Sw. A possible explanation for this is that starch granules present in the films (Fig. 2B) slowed down the access of water molecules to the polymer matrix.

Table 2

The effect of Astasana (AST) concentration on the pH of film-forming solutions (FFSs), puncture strength (PS), puncture deformation (PD), contact angle (CA), swelling (Sw), and water vapour permeability (WVP), of the 75/25 carboxymethyl cellulose/gelatin (CMC75/GEL25) and 75/25 octenyl succinic anhydride starch/gelatin (OSA75/GEL25) films.

Film	AST (%)	pH of FFSs	PS (MPa)	PD (mm)	CA (°)	Sw (%)	WVP (°)
CMC75/ GEL25	0	6.35	11.80	5.55	69.2	831.60	51.07
		±	±	±	±	±	±
		0.02 ^f	1.34 ^c	0.34 ^{ab}	0.42 ^{cd}	28.68 ^e	1.07 ^a
	0.25	6.26	9.43	7.16	47.25	557.58	51.25
		±	±	±	±	±	±
		0.03 ^e	1.00 ^b	0.96 ^c	0.35 ^a	21.47 ^d	1.13 ^{ab}
	0.5	6.29	8.67	6.78	55.50	557.06	52.20
		±	±	±	±	±	±
		0.01 ^e	0.83 ^b	0.69 ^{bc}	0.71 ^b	11.03 ^d	1.73 ^{ab}
	1	6.10	8.75	5.40	63.25	524.76	52.09
		±	±	±	±	±	±
		0.01 ^d	0.45 ^b	0.71 ^a	1.77 ^c	22.64 ^c	1.74 ^{ab}
OSA75/ GEL25	0	4.89	2.20	14.85	64.25	146.17	54.27
		±	±	±	±	± 4.35 ^a	±
		0.01 ^c	0.29 ^a	1.11 ^d	1.06 ^c	0.61 ^b	
	0.25	4.86	1.96	14.95	68.40	186.51	52.25
		±	±	±	±	± 3.45 ^b	±
		0.00 ^b	0.09 ^a	1.11 ^d	0.85 ^c	2.44 ^{ab}	
	0.5	4.85	2.16	14.74	64.25	178.27	51.92
		±	±	±	±	±	±
		0.01 ^b	0.22 ^a	0.73 ^d	1.06 ^c	14.00 ^b	0.52 ^{ab}
	1	4.80	2.32	14.50	73.09	182.45	51.11
		±	±	±	±	±	±
		0.01 ^a	0.17 ^a	1.05 ^d	2.83 ^d	10.17 ^b	1.82 ^{ab}

^{a-f} Values with the different superscript letters within one column are significantly different ($p < 0.05$).

^a ($\text{g mm m}^{-2} \text{d}^{-1} \text{kPa}^{-1}$).

Moreover, it can be hypothesised that AST components may have interfered with the polymer network packaging, e.g. through the development of polymer-ASX hydrogen bonds (Liu et al., 2020), which inhibited the formation of polymer-water hydrogen bonds and consequently resulted in limited water absorption ability.

Contrary to the CMC-based system, the AST increased the Sw value in the OSA-containing film (Table 2). This result is difficult to explain, but it might be related to the initially low Sw of the OSA75/GEL25 system. It is possible that, in this case, the AST ingredients caused the films to be more porous (less coherent), thus larger amounts of water molecules were immobilised in the film matrix.

All the films obtained were totally water-soluble (Fig. 4). This outcome is in contrast to results reported in previous studies (Kowalczyk, Pytka, et al., 2020; Lupina et al., 2019), which demonstrated incomplete solubility of the polysaccharide75/GEL25 systems. This inconsistency may be easily explained by the differences in the sample incubation conditions (30 °C vs. 25 °C), i.e. the temperature closer to the GEL melting point (~32 °C) (Ninan, Joseph, & Aliyamveetil, 2014) favoured the dissolution of the samples. A comparison between the control samples showed that the time required for 100% solubility of the CMC- and OSA-containing films were ~10 min. The initial dissolution profiles (up to 5 min) revealed that the CMC-based films were more soluble than the OSA-containing samples. The strong affinity of the CMC-based film for water (the highest Sw and the fastest solubility) could be explained by the presence of numerous hydrophilic carboxyl groups in the polymer (Kowalczyk & Baraniak, 2014). The presence of the AST in the OSA-containing films reduced the TSM (Fig. 4), which might be related to the fact that insoluble starch granules hindered the penetration of water molecules between the polymeric network. It should be mentioned here that, although 100% solubility was estimated for the AST-supplemented OSA-based films, the visual observations of the aqueous medium revealed that the samples were not fully solubilised but disintegrated into small-size insoluble particles, which were

sediment-prone (Fig. S2). Nevertheless, in the TSM test, these particles were considered as the dissolved fraction. In general, the higher the AST content, the lower the solubility was observed. It was found that the AST was ineffective in the reduction of the TSM of CMC-containing film. A similar result was reported for CMC films incorporated with candelilla wax (Kowalczyk & Baraniak, 2014). This indicates that it is difficult to reduce the water affinity of such a rapidly soluble material as CMC. Interestingly, this study showed that the AST acted as a solubility enhancer for the CMC-based film (Fig. 4); however, an increase in the AST concentration resulted in less soluble films.

It should be noted here, that the TSM results partially support the findings of CA analyses; i.e. the AST increased wettability and, consequently, the solubility of the CMC-based carrier, while the opposite possibility was observed for the OSA-based film (Table 2, Fig. 4).

In summary, the differential effect of AST on the CA, Sw, and TSM of CMC- and OSA-containing films suggests that native starch could show both binder and disintegrant action in a carrier (Builders & Arhewoh, 2016).

3.6. Water vapour/oxygen barrier properties

The comparison of the WVP values revealed that the control CMC75/GEL25 film exhibited slightly better water vapour barrier properties than the control OSA75/GEL25 carrier (51.07 vs. 54.27 $\text{g mm m}^{-2} \text{d}^{-1} \text{kPa}^{-1}$, Table 2). A possible explanation for this might be that the CMC-based film, due to its excellent water absorption capacity (Table 2), could just immobilize passing aqueous vapour, thus WVP seemed reduced. The incorporation of AST did not affect the WVP of the films. This outcome is contrary to that of Gomez-Estela et al. (2015). As mentioned in Section 1, the decrease in WVP observed by the cited authors was primarily due to the incorporation of the oil phase (used for extraction of ASX from shrimp wastes) into the film matrix. In accordance with the present results, a previous study (Queiroz Assis, D'Angelo Rios, de Oliveira Rios, & Olivera, 2020) has demonstrated that the presence of norbixin (a water-soluble carotenoid) at the level of 0.03–0.05% had no significant effect on the WVP of cellulose acetate film; nevertheless, the bulky amounts of the carotenoid (0.1%) contributed to a greater diffusion of water vapour through the film.

Table 3 demonstrates the OTR of the CMC75/GEL25 films (control and film containing the maximum level of AST). Unfortunately, it was impossible to obtain reliable data on the OTR of the OSA75/GEL25 films. The reason was a significant deformation of the films during the test; i.e. the samples were extremely stretched under the gas flow and, consequently, clogged the oxygen detector of the instrument. It was found that the incorporation of AST resulted in about a 5-fold reduction in OTR of the CMC-based film. It clearly shows that AST contains sealing and/or oxygen scavenging agents. It is possible that the starch granules and/or ASX molecules, acting as a filler between the immiscible polymer phases, hindered the oxygen molecules permeation across the non-homogenous blend matrix. Moreover, results from previous studies showed the incorporation of ascorbic acid and its salts (Brody, Strupinsky, & Kline, 2001; Janjarasskul, Min, & Krochta, 2013) or tocopherol (Scarfato, Avallone, Galdi, Di Maio, & Incarnato, 2015), i.e. the antioxidants that are present in the AST formulation, can induce the oxygen-scavenging function of the biopolymeric materials.

3.7. Release of AST

The preliminary release tests (data not shown) and other research (Colín-Chávez, Soto-Valdez, Peralta, Lizardi-Mendoza, & Balandrán-Quintana, 2013a) have shown that the migration of the ASX from the polymeric carriers to the acceptor solution at 25 °C is a several-day long process. Therefore, in this work, accelerated release testing conditions with elevated temperature (30 °C) were employed. Fig. 5 and Fig. S3 show cumulative (mg/cm^2) and percentage amounts of AST released from the composite films as a function of time, respectively. Depending

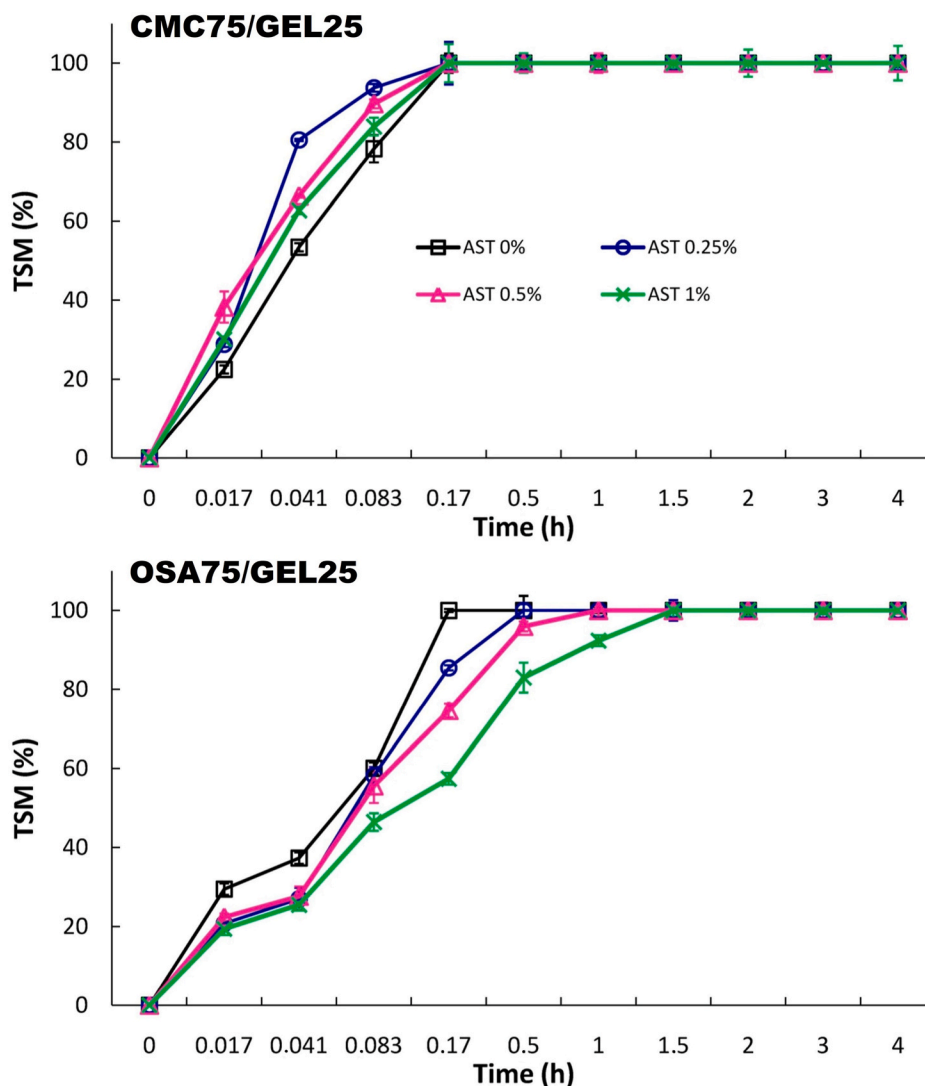


Fig. 4. Effect of increasing Astasana (AST) concentration on the kinetics of total soluble matter (TSM) of the 75/25 carboxymethyl cellulose/gelatin (CMC75/GEL25) and 75/25 octenyl succinic anhydride starch/gelatin (OSA75/GEL25) films.

Table 3

The effect of Astasana (AST) addition on the oxygen transmission rate (OTR) of the 75/25 carboxymethyl cellulose/gelatin (CMC75/GEL25) and 75/25 octenyl succinic anhydride starch/gelatin (OSA75/GEL25) films.

Films	AST (%)	OTR ($\text{cm}^3 \mu\text{m}/(\text{m}^2 \text{d})$)
CMC75/GEL25	0	$174.12 \pm 24.83^{\text{b}}$
	1	$34.06 \pm 7.25^{\text{a}}$
OSA75/GEL25	0	n.d.
	1	n.d.

^{a-f} Values with the different superscript letters within one column are significantly different ($p < 0.05$).

n.d. – no data (the films were deformed during the test and clogged the oxygen detector of the instrument).

on the carrier type and AST concentration, ~35–100% of the AST was released from the films during the 4-h dissolution test. Since the release of AST from the OSA75/GEL25 carrier was incomplete, it was impossible to predict the $t_{50\%}$ for the 0.5%AST- and 1%AST-supplemented systems. The $t_{25\%}$ values ranged from 1.20 to 19.86 min (Table 4). The rapid diffusion process ('burst effect') was observed for the CMC-containing films ($t_{25\%} = 1.20$ – 1.74 min). This finding is consistent with that reported by Kowalczyk, Pytko, et al. (2020), who analysed the

migration of iso- α -acids from films based on the CMC/GEL blends. These results are likely to be related to the fast disintegration of the bi-polymeric matrix in contact with water (Fig. 4). In the case of the OSA-based carrier, the lag time was observed for the AST release (Fig. 5). The comparison of the $t_{25\%}$ values showed that, at the 1% AST incorporation level, the OSA-based film exhibited more than 10 times slower release of AST compared to the CMC-based carrier. As suggested by Zhao et al., (2019), the incomplete release of AST from the OSA/GEL system (~35–63%, depending on the AST concentration (Fig. S3)) may be related to the partial encapsulation of this carotenoid in the complex bi-polymeric coacervates. As mentioned previously, the AST-supplemented OSA75/GEL25 films did not dissolve completely, i.e. they were disintegrated into fine solid particles (Fig. S2). This finding is partially consistent with that shown by Wu and McClements (2015), who observed that mixing of OSA with GEL resulted in hydrogel particles with a mean diameter ranging from 5 to 13 μm . Therefore, it is possible that, despite the complete erosion of the film matrix, the AST was permanently immobilised in the hydrogel coacervates and, therefore, the release process reached a plateau, although it was incomplete (Fig. 5; Fig. S3). Wu and McClements (2015) suggested that OSA/GEL coacervates may be used to encapsulate functional ingredients. The result of the present work indirectly confirms this assumption.

In contrast to the CMC-based carrier, the increasing AST

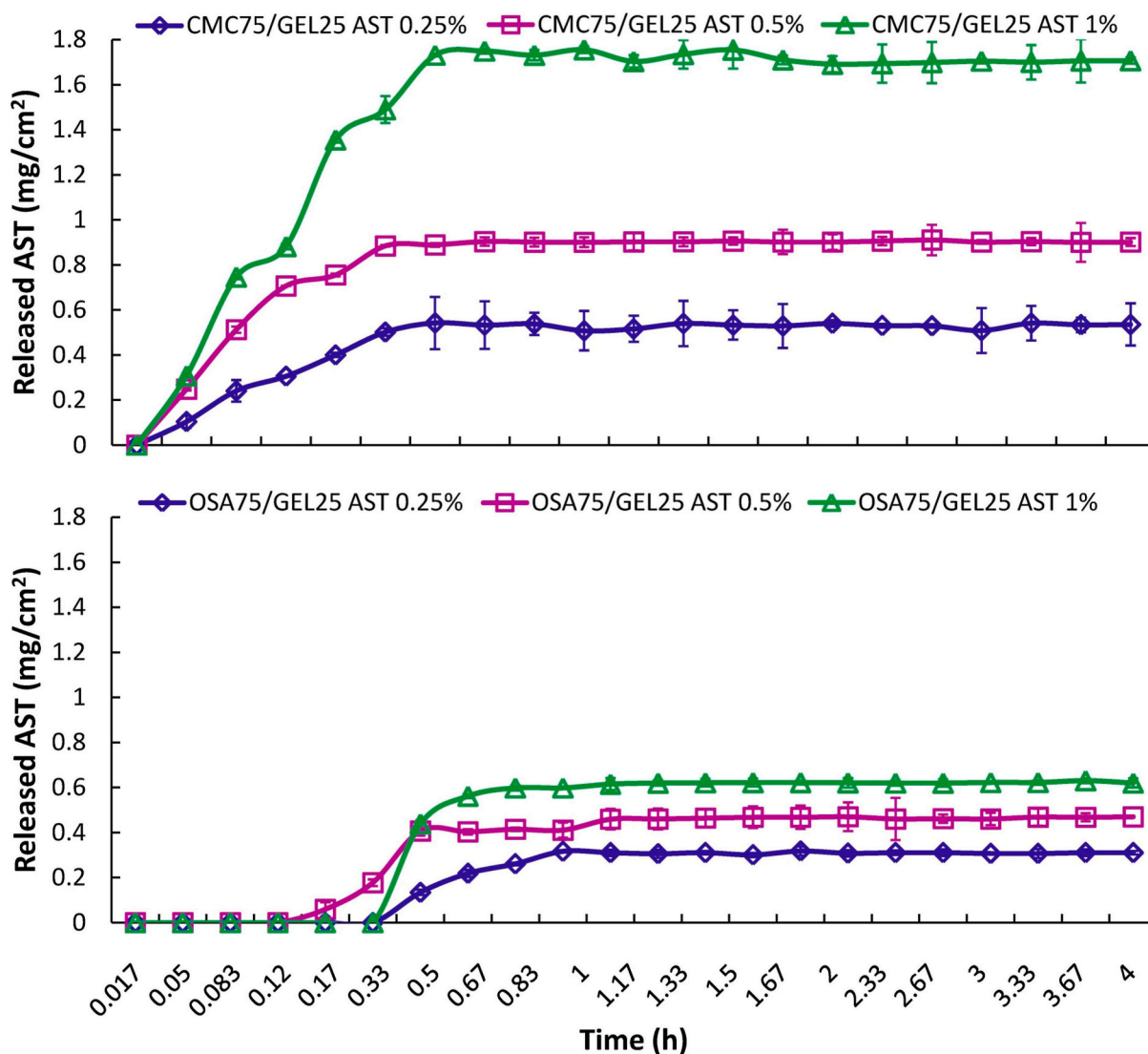


Fig. 5. Kinetics of cumulative release (mg/cm²) of Astasana (AST) from the 75/25 carboxymethyl cellulose/gelatin (CMC75/GEL25) and 75/25 octenyl succinyl anhydride starch/gelatin (OSA75/GEL25) blend films.

Table 4

Times required for 25% ($t_{25\%}$) and 50% ($t_{50\%}$) Astasana (AST) release from the 75/25 carboxymethyl cellulose/gelatin (CMC75/GEL25) and 75/25 octenyl succinyl anhydride starch/gelatin (OSA75/GEL25) films obtained from the best fitting mathematical models.

Film	AST (%)	$t_{25\%}$ (min)	$t_{50\%}$ (min)
CMC75/GEL25	0	–	–
	0.25	1.56 ^(Ho)	3.48 ^(Ho)
	0.5	1.20 ^(F-O Fmax)	2.88 ^(F-O Fmax)
	1	1.74 ^(Ho)	4.08 ^(Ho)
OSA75/GEL25	0	–	–
	0.25	20.04 ^(Pr2)	33.9 ^(Pr2)
	0.5	12.36 ^(Lo2)	n.d. ^(Lo2)
	1	19.86 ^(P-S Tlag)	n.d. ^(P-S Tlag)

(F-O Fmax) First order with F_{max} model.

(Ho) Korsmeyer–Peppas with T_{lag} model.

(P-S Tlag) Peppas–Sahlin 1 with T_{lag} model.

(Lo 2) Logistic 2 model.

(Pr 2) Probit 2 model.

n.d. – no data.

concentration tended to slow down the release rate in the OSA-based system (Fig. S3; Table 4), which could be explained by the gradually decreasing solubility (Fig. 4). As can be seen from Fig. S4, there was a strong positive correlation ($R^2 = 0.78$) between the AST release rate and the TSM. Since the AST concentration strongly affected the release profiles, various mathematical models were required to predict the rate of AST release from the CMC- and OSA-based films (Fig. 6).

Eight mathematical equations (Table S1) were used for the quantitative interpretation of the data obtained from the ASTA release assay. The $R^2_{adjusted}$ and parameter values estimated for the models are presented in Tables S2, S3, and S4. It was impossible to fit one optimal model to describe the migration of AST from the particular carrier types; however, based on $R^2_{adjusted}$ averages, the Probit 2 (Pr 2) model provided the best fit for all release series data ($R^2_{adjusted}$ mean = 0.9915). It was found that, in the case of the CMC-based carrier, two-parameter models: First order with F_{max} (F-O F_{max}) and Hopfenberg (Ho) approximated the experimental points better than the three- and four-parameter equations (Table S2). A possible explanation for this result may be the lack of time lag for these systems. The F-O model describes the dissolution of a drug that is not effectively enclosed in the polymeric matrix and is ready to dissolve from the carrier surface intermediately after contact with the release medium. In turn, the Ho model correlates the

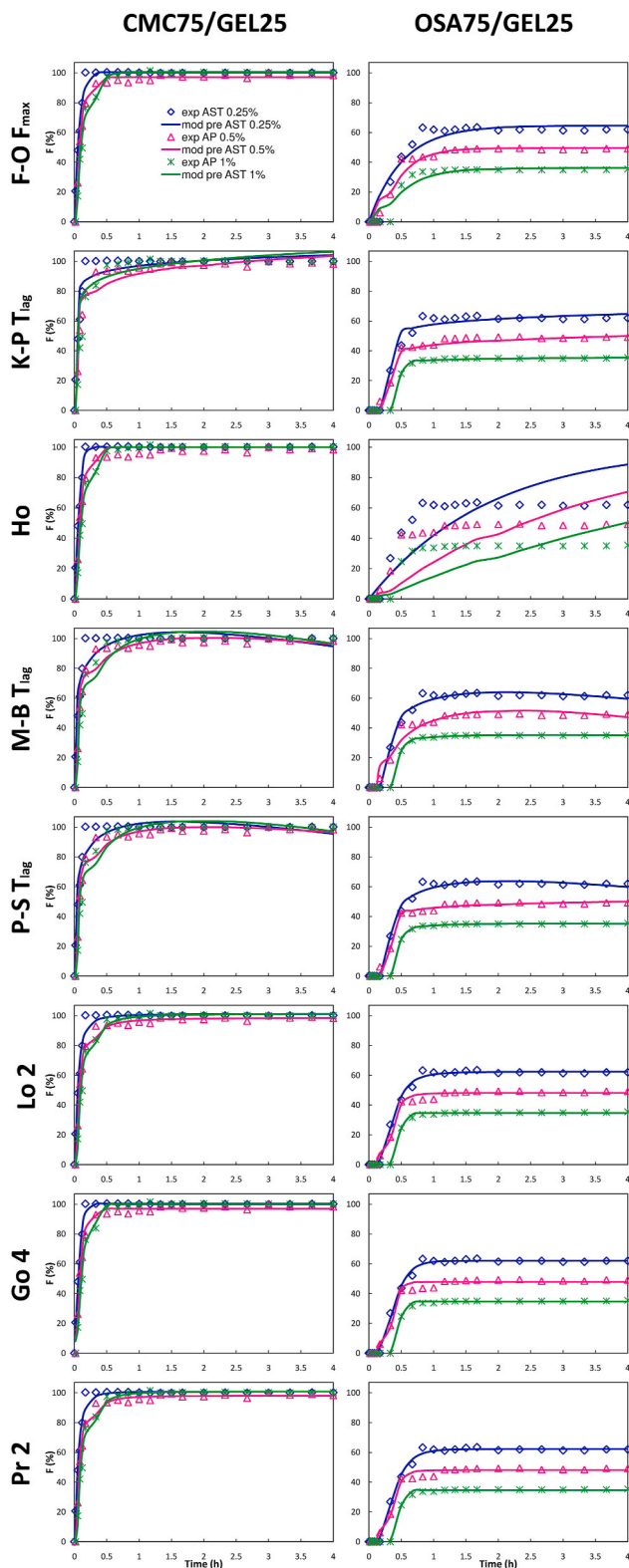


Fig. 6. Fraction (F) of Astasana (AST) released from the 75/25 carboxymethyl cellulose/gelatin (CMC75/GEL25) and 75/25 octenyl succinic anhydride starch/gelatin (OSA75/GEL25) films according to the First order with F_{max} ($F-O F_{max}$), Korsmeyer–Peppas with T_{lag} (K–P T_{lag}), Hopfenberg (Ho), Makoid–Banakar with T_{lag} (M–B T_{lag}), Peppas–Sahlin 1 with T_{lag} (P–S T_{lag}), Logistic 2 (Lo 2), Gompertz 4 (Go 4), and Probit 2 (Pr 2) models; experimental (points) and theoretical data (lines).

substance release from surface eroding polymers (Paarakh, Jose, Setty, & Peter, 2018). The Ho model, for example, has been used for successful modeling the release of amoxicillin from erodible hydroxypropyl methylcellulose tablets (Katzhendler, Hoffman, Goldberger, & Friedman, 1997). The release profile obtained for the OSA-based system was an “S-shaped” curve (Fig. 5; Fig. S3). Consequently, in the case of this carrier system, the more complex models (i.e. with at least three parameters) approximated the experimental points better than the two-parameter ones (Table S2).

According to the Korsmeyer–Peppas with T_{lag} (K–P T_{lag}) model, the n values were below 0.5 ($n = 0.006–0.082$, Table S4), which shows that the AST was transported via a quasi-Fickian diffusion-controlled mechanism (Malekjani & Jafari, 2021). This finding is consistent with that reported by Colín-Chávez et al., (2013a), who analysed the diffusion of natural ASX from polyethylene active packaging films into ethanol.

3.8. Antioxidant properties

So far, ASX has two main potential technological applications, i.e. in food colouring and antioxidant protection. It was found that the control polysaccharide/GEL films (without AST) showed relatively high ABTS⁺⁺ scavenging activity (~62–77% at 180 min of incubation; Fig. 7). Since the films based only on the polysaccharides have poor antioxidant potential (Kowalczyk & Biendl, 2016), this result may be ascribed to the presence of the GEL fraction in the carriers. As suggested previously (Kowalczyk et al., 2021), some amino acid residues of GEL (including glycine and proline) could donate electrons and neutralise free radicals. The control CMC-based film exhibited higher antiradical ability than the OSA-based carrier, which might be related to its faster initial dissolution (Fig. 7). As expected, the increasing level of AST in the films resulted in a gradual increase in the ABTS⁺⁺ scavenging capacity (Fig. 7). The CMC75/GEL25 system, regardless of the AST concentration, offered higher antioxidant activity than the OSA75/GEL25 film. This result can be explained in terms of the release profiles of the films (Fig. 5). As can be seen from Table S5, a high positive correlation was found between the cumulative AST release (mg/cm^2) and the ABTS scavenging ($R^2 = 0.78–0.91$).

4. Conclusion

Although CMC75/GEL25 and OSA75/GEL25 are immiscible phase-separated systems, they possess good film-forming abilities. The comparison of the physicochemical properties of the films revealed that the AST-supplemented CMC75/GEL25 and OSA75/GEL25 films had similar color; nevertheless, the CMC-containing films were stronger, less stretchable, and more opaque, than the OSA-based films. A five-fold decrease in the oxygen permeability of the CMC75/GEL25 film, as a result of AST incorporation (at a level of 1%) was observed. It suggests that the obtained film could protect the food against oxidation as effective oxygen barrier material.

The droplet-type microstructures (likely coacervates) formed by the OSA-based system showed the AST encapsulation efficiency, as indicated by the incomplete AST release (with a lag time) and the particle sedimentation behaviour. The slower release of AST from the OSA-based carrier, compared to the CMC-containing systems, was mainly influenced by its slower initial dissolution rate. Nevertheless, the sigmoid release profile observed for the OSA-containing carrier might be considered beneficial. It can be assumed that when this system is used as the coating material for high-moisture food, the major dose of the antioxidant will be maintained on the food surface, where the oxidation reactions mainly occur. In turn, the released AST fraction will inhibit oxidation in the surface layer of the product, which is also favourable. By that logic, the rapid release (‘burst effect’) of AST from the CMC75/GEL25 carrier is not advantageous, as it may lead to quick depletion of the protective action of the antioxidant on the surface.

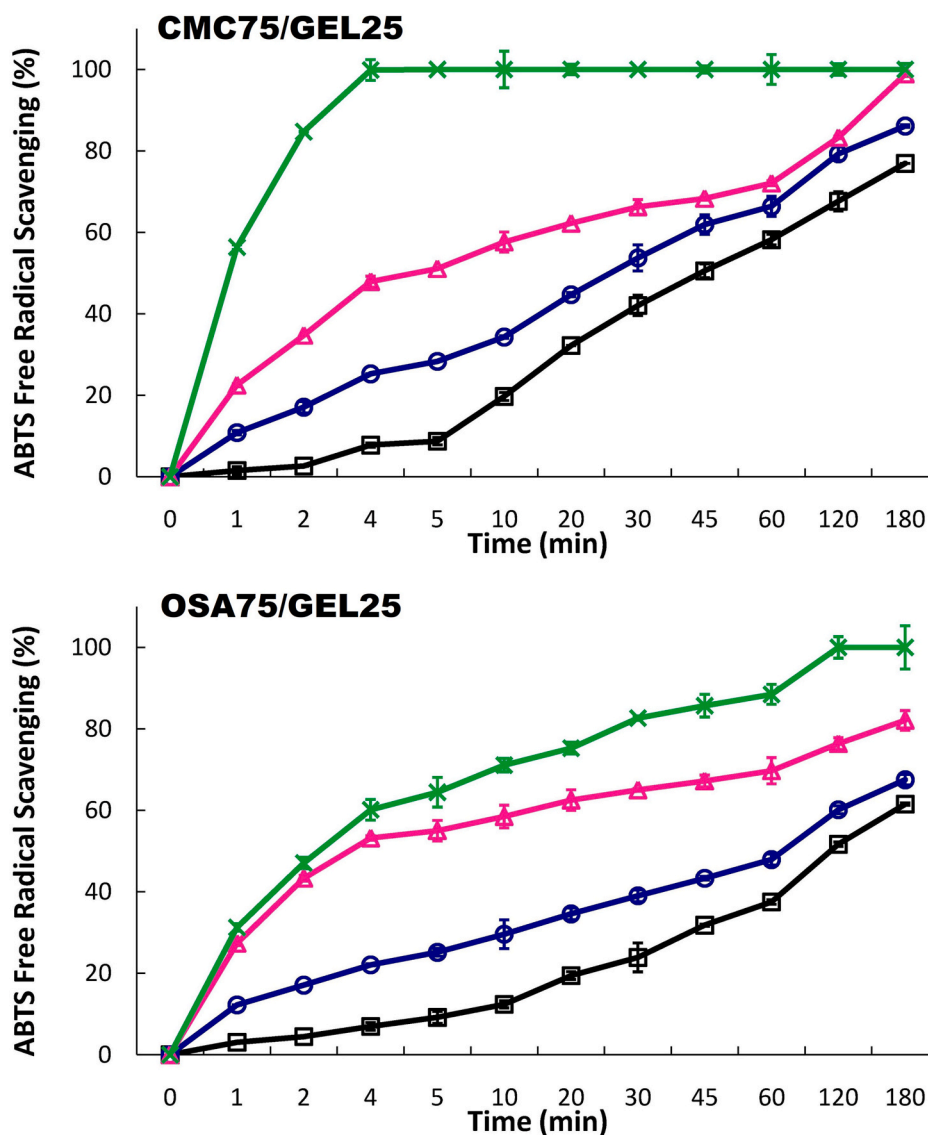


Fig. 7. Effect of increasing Astasana (AST) concentration on the kinetics of antiradical activity of the 75/25 carboxymethyl cellulose/gelatin (CMC75/GEL25) and 75/25 octenyl succinic anhydride starch/gelatin (OSA75/GEL25) films.

In summary, the 1%AST-supplemented OSA75/GEL25 films offered controlled diffusion-limited release and simultaneously maximised the antioxidant potential of AST. The AST-added films, owing to their red color, good oxygen barrier and enhanced free radical scavenging properties could be a preferred choice for the active antioxidant packaging development for specific applications, e.g. edible coatings for cheese, nuts, red meat, surimi sticks, etc.

CRedit authorship contribution statement

Katarzyna Łupina: Conceptualization, Methodology, Data curation, Formal analysis, Visualization, Investigation, Writing – original draft. **Dariusz Kowalczyk:** Conceptualization, Methodology, Supervision, Validation. **Magdalena Lis:** Investigation. **Aneta Raszewska-Kaczor:** Investigation. **Emilia Droźłowska:** Investigation.

Declaration of competing interest

The authors declare that they have no known competing financial interests or personal relationships that could have appeared to influence the work reported in this paper.

Acknowledgements

This work was financially supported by the National Science Centre (Poland) under grant number 2019/35/N/NZ9/01795. We thank Emil Zięba (Laboratory of Confocal and Electron Microscopy, Centre for Interdisciplinary Research Faculty of Science and Health, John Paul II Catholic University of Lublin, Konstantynów 1J, 20–708 Lublin, Poland) for assistance with cryo-SEM observation of the samples.

Appendix A. Supplementary data

Supplementary data to this article can be found online at <https://doi.org/10.1016/j.foodhyd.2021.107179>.

List of abbreviations

ABTS	2,2'-azino-bis(3-ethylbenzothiazoline-6-sulfonic acid) diammonium salt
AST	AstaSana™ 5% CWS/S-TG; ASX-astaxanthin
ATR-FTIR	attenuated total reflection Fourier transform infrared
CA	contact angle

CDX–085	Cardax's proprietary astaxanthin prodrug
CMC	carboxymethyl cellulose
cryo-SEM	cryogenic scanning electron microscopy
DDA	disodium disuccinate astaxanthin
EFSA	European Food Safety Authority
FFS	film-forming solution
F-O F_{max}	First order with F _{max} model
GEL	gelatin
Go 4	Gompertz 4 model
Ho	Hopfenberg model
K-P T_{lag}	Korsmeyer–Peppas with time lag model
Lo 2	Logistic 2 model
RH	relative humidity
M-B T_{lag}	Makoid–Banakar with time lag model
Op	opacity
OSA	octenyl succinic anhydride starch
OTR	oxygen transmission rate
PD	puncture deformation
Pr 2	Probit 2 model
PS	puncture strength
P-S T_{lag}	Peppas–Sahlin 1 with time lag model
SEM	scanning electron microscopy
Sw	swelling
TSM	total soluble matter
WVP	water vapour permeability

References

- Ačkar, D., Babić, J., Jozinović, A., Miličević, B., Jokić, S., Miličević, R., Jokić, S., & Šubarić, D. (2015). Starch modification by organic acids and their derivatives: A review. *Molecules*, 20(10), 19554–19570. <https://doi.org/10.3390/molecules201019554>
- Ambati, R. R., Moi, P. S., Ravi, S., & Aswathanarayana, R. G. (2014). Astaxanthin: Sources, extraction, stability, biological activities and its commercial applications - a review. *Marine Drugs*, 12(1), 128–152. <https://doi.org/10.3390/md12010128>
- Bogacz-Radomska, L., & Harasym, J. (2018). β -Carotene-properties and production methods. *Food Quality and Safety*, 2(2), 69–74. <https://doi.org/10.1093/fqsafe/fyy004>
- Bourtoom, T. (2008). Edible films and coatings : Characteristics and properties. *International Food Research Journal*, 15(3), 237–248.
- Brendler, T., & Williamson, E. M. (2019). Astaxanthin: How much is too much? A safety review. *Phytotherapy Research*, 33(12), 3090–3111. <https://doi.org/10.1002/ptr.6514>
- Brody, A., Strupinsky, E., & Kline, L. (2001). *Active packaging for food applications*. Boca Raton: CRC Press.
- Builders, P. F., & Arhewoh, M. I. (2016). Pharmaceutical applications of native starch in conventional drug delivery. *Starch/Stärke*, 68, 864–873. <https://doi.org/10.1002/star.201500337>
- Capelli, B., Bagchi, D., & Cysewski, G. R. (2013). Synthetic astaxanthin is significantly inferior to algal-based astaxanthin as an antioxidant and may not be suitable as a human nutraceutical supplement. *Nutrafods*, 12(4), 145–152. <https://doi.org/10.1007/s13749-013-0051-5>
- Coates, J. (2006). Interpretation of infrared spectra, A practical approach. In R. Meyers (Ed.), *Encyclopedia of analytical chemistry* (pp. 1–23). John Wiley & Sons, Ltd. <https://doi.org/10.1002/9780470027318.a5606>
- Colín-Chávez, C., Soto-Valdez, H., Peralta, E., Lizardi-Mendoza, J., & Balandrán-Quintana, R. (2013a). Diffusion of natural astaxanthin from polyethylene active packaging films into a fatty food simulant. *Food Research International*, 54(1), 873–880. <https://doi.org/10.1016/j.foodres.2013.08.021>
- Colín-Chávez, C., Soto-Valdez, H., Peralta, E., Lizardi-Mendoza, J., & Balandrán-Quintana, R. (2013b). Fabrication and properties of antioxidant polyethylene-based films containing marigold (*Tagetes erecta*) extract and application on soybean oil stability. *Packaging Technology and Science*, 29, 399–412. <https://doi.org/10.1002/pts>
- EFSA. (2014). Panel on dietetic products, Nutrition and Allergies (NDA) Scientific opinion on the safety of astaxanthin-rich ingredients (AstaREAL A1010 and AstaREAL L10) as novel food ingredients. *EFSA Journal*, 3757, 1–35.
- Feng, Z. Z., Li, M. Y., Wang, Y. T., & Zhu, M. J. (2018). Astaxanthin from *Phaffia rhodozyma*: Microencapsulation with carboxymethyl cellulose sodium and microcrystalline cellulose and effects of microencapsulated astaxanthin on yogurt properties. *Lebensmittel-Wissenschaft & Technologie*, 96, 152–160. <https://doi.org/10.1016/j.lwt.2018.04.084>
- Gómez-Estaca, J., Calvo, M. M., Sánchez-Faure, A., Montero, P., & Gómez-Guillén, M. C. (2015). Development, properties, and stability of antioxidant shrimp muscle protein films incorporating carotenoid-containing extracts from food by-products. *Lebensmittel-Wissenschaft & Technologie*, 64(1), 189–196. <https://doi.org/10.1016/j.lwt.2015.05.052>
- Han, & Floros, J. D. (1997). Casting antimicrobial packaging films and measuring their physical properties and antimicrobial activity. *Journal of Plastic Film and Sheeting*, 13(4), 287–298. <https://doi.org/10.1177/875608799701300405>
- Hejna, A., Lenža, J., Formela, K., & Korol, J. (2019). Studies on the combined impact of starch source and multiple processing on selected properties of thermoplastic starch/ethylene-Vinyl acetate blends. *Journal of Polymers and the Environment*, 27(5), 1112–1126. <https://doi.org/10.1007/s10924-019-01406-1>
- Higuera-Ciajara, I., Félix-Valenzuela, L., & Goycoolea, F. M. (2006). Astaxanthin: A review of its chemistry and applications. *Critical Reviews in Food Science and Nutrition*, 46(2), 185–196. <https://doi.org/10.1080/10408690590957188>
- ISO 2528. (1995). *Sheet materials - determination of water vapour transmission rate - gravimetric (dish) method*.
- Jafari, J., Emami, S. H., Samadikuchaksaraei, A., Bahar, M. A., & Gorjipour, F. (2011). Electrospun chitosan-gelatin nanofibrous scaffold: Fabrication and in vitro evaluation. *Bio-Medical Materials and Engineering*, 21(2), 99–112. <https://doi.org/10.3233/BME-2011-0660>
- Janjarasskul, T., Min, S. C., & Krochta, J. M. (2013). Triggering mechanisms for oxygen-scavenging function of ascorbic acid-incorporated whey protein isolate films. *Journal of the Science of Food and Agriculture*, 93(12), 2939–2944. <https://doi.org/10.1002/jsfa.6120>
- Katzhendler, I., Hoffman, A., Goldberger, A., & Friedman, M. (1997). Modeling of drug release from erodible tablets. *Journal of Pharmaceutical Sciences*, 86(1), 110–115. <https://doi.org/10.1021/js9600538>
- Kowalczyk, D., & Baraniak, B. (2014). Effect of candelilla wax on functional properties of biopolymer emulsion films - a comparative study. *Food Hydrocolloids*, 41, 195–209. <https://doi.org/10.1016/j.foodhyd.2014.04.004>
- Kowalczyk, D., & Biendl, M. (2016). Physicochemical and antioxidant properties of biopolymer/candelilla wax emulsion films containing hop extract - a comparative study. *Food Hydrocolloids*, 60, 384–392. <https://doi.org/10.1016/j.foodhyd.2016.04.010>
- Kowalczyk, D., Kordowska-Wiater, M., Karaś, M., Zięba, E., Mężyńska, M., & Wiącek, A. E. (2020). Release kinetics and antimicrobial properties of the potassium sorbate-loaded edible films made from pullulan, gelatin and their blends. *Food Hydrocolloids*, 101, 105539. <https://doi.org/10.1016/j.foodhyd.2019.105539>
- Kowalczyk, D., Pytka, M., Szymanowska, U., Skrzypek, T., Lupina, K., & Biendl, M. (2020). Release kinetics and antibacterial activity of potassium salts of iso- α -acids loaded into the films based on gelatin, carboxymethyl cellulose and their blends. *Food Hydrocolloids*, 109, 106104. <https://doi.org/10.1016/j.foodhyd.2020.106104>
- Kowalczyk, D., Szymanowska, U., Skrzypek, T., Basiura-Cembala, M., Lupina, K., & Biendl, M. (2021). Edible films based on gelatin, carboxymethyl cellulose, and their blends as carriers of potassium salts of iso- α -acids: Structural, physicochemical and antioxidant properties. *Food Hydrocolloids*, 115. <https://doi.org/10.1016/j.foodhyd.2020.106574>. December 2020.
- Liu, Y., Huang, L., Li, D., Wang, Y., Chen, Z., Zou, C., Liu, W., Ma, Y., Cao, M. J., & Liu, G. M. (2020). Re-assembled oleic acid-protein complexes as nano-vehicles for astaxanthin: Multispectral analysis and molecular docking. *Food Hydrocolloids*, 103. <https://doi.org/10.1016/j.foodhyd.2020.105689>. January.
- Liu, C., Zhang, S., McClements, D. J., Wang, D., & Xu, Y. (2019). Design of astaxanthin-loaded core-shell nanoparticles consisting of chitosan oligosaccharides and poly(lactic-co-glycolic acid): Enhancement of water solubility, stability, and bioavailability. *Journal of Agricultural and Food Chemistry*, 67(18), 5113–5121. <https://doi.org/10.1021/acs.jafc.8b06963>
- Malekjani, N., & Jafari, S. M. (2021). Modeling the release of food bioactive ingredients from carriers/nanocarriers by the empirical, semiempirical, and mechanistic models. *Comprehensive Reviews in Food Science and Food Safety*, 20(1), 3–47. <https://doi.org/10.1111/1541-4337.12660>
- Martínez-Delgado, A. A., Khandual, S., & Villanueva-Rodríguez, S. J. (2017). Chemical stability of astaxanthin integrated into a food matrix: Effects of food processing and methods for preservation. *Food Chemistry*, 225, 23–30. <https://doi.org/10.1016/j.foodchem.2016.11.092>
- Meléndez Martínez, A. J., Vicario Romero, I., & Heredia Mira, F. J. (2004). Estabilidad de los pigmentos carotenoides en los alimentos. *Archivos Latinoamericanos de Nutrición*, 54(2).
- Ninan, G., Joseph, J., & Aliyamveetil, Z. A. (2014). A comparative study on the physical, chemical and functional properties of carp skin and mammalian gelatins. *Journal of Food Science & Technology*, 51(9), 2085–2091. <https://doi.org/10.1007/s13197-012-0681-4>
- Paarakh, M. P., Jose, P. A. N., Setty, C. M., & Peter, G. V. (2018). Release kinetics – concepts and applications. *International Journal of Pharmacy Research & Technology*, 8(1), 12–20. <https://doi.org/10.31838/ijprt/08.01.02>
- Panis, G., & Carreon, J. R. (2016). Commercial astaxanthin production derived by green alga *Haematococcus pluvialis*: A microalgae process model and a techno-economic assessment all through production line. *Algal Research*, 18, 175–190. <https://doi.org/10.1016/j.algal.2016.06.007>
- Queiroz Assis, R., D'Angelo Rios, P., de Oliveira Rios, A., & Olivera, F. C. (2020). Biodegradable packaging of cellulose acetate incorporated with norbixin, lycopene or zeaxanthin. *Industrial Crops and Products*, 147, 112212. <https://doi.org/10.1016/j.indcrop.2020.112212>
- Santos-Sánchez, N. F., Hernández-Carlos, B., Torres-Ariño, A., & Salas-Coronado, R. (2020). Astaxanthin and its formulations as potent oxidative stress inhibitors. *Pharmacology Reviews*, 14(27), 8–15.
- Scarfato, P., Avallone, E., Galdi, M. R., Di Maio, L., & Incarnato, L. (2015). Preparation, characterization, and oxygen scavenging capacity of biodegradable a-tocopherol/PLA microparticles for active food packaging applications. *Polymer Composites*, 38(5), 981–986. <https://doi.org/10.1002/pc>

- Shah, M. M. R., Liang, Y., Cheng, J. J., & Daroch, M. (2016). Astaxanthin-producing green microalga *Haematococcus pluvialis*: From single cell to high value commercial products. *Frontiers in Plant Science*, 7, 1–28. <https://doi.org/10.3389/fpls.2016.00531>
- Sieradzka, M., & Kolodziejczyk-Czepas, J. (2016). Astaksantyna-karotenoidowy przeciwutleniacz o właściwościach kardioprotekcyjnych Astaxanthin-a carotenoid antioxidant with cardioprotective properties. *Problemy Higieny i Epidemiologii*, 97(3), 197–206.
- Stahl, W., & Sies, H. (2003). Antioxidant activity of carotenoids. *Molecular Aspects of Medicine*, 24(6), 345–351. [https://doi.org/10.1016/S0098-2997\(03\)00030-X](https://doi.org/10.1016/S0098-2997(03)00030-X)
- Tesch, S., Gerhards, C., & Schubert, H. (2002). Stabilization of emulsions by OSA starches. *Journal of Food Engineering*, 54(2), 167–174. [https://doi.org/10.1016/S0260-8774\(01\)00206-0](https://doi.org/10.1016/S0260-8774(01)00206-0)
- Wu, B., & McClements, D. (2015). Microgels formed by electrostatic complexation of gelatin and OSA starch: Potential fat or starch mimetics. *Food Hydrocolloids*, 47, 87–93. <https://doi.org/10.1016/j.foodhyd.2015.01.021>
- Ye, K. X., Fan, T. T., Keen, L. J., & Han, B. N. (2019). A review of pigments derived from marine natural products. *Israel Journal of Chemistry*, 59(5), 327–338. <https://doi.org/10.1002/ijch.201800154>
- Yuan, C., Jin, Z., & Xu, X. (2012). Inclusion complex of astaxanthin with hydroxypropyl- β -cyclodextrin: UV, FTIR, ¹H NMR and molecular modeling studies. *Carbohydrate Polymers*, 89(2), 492–496. <https://doi.org/10.1016/j.carbpol.2012.03.033>
- Zhang, Y., Huo, M., Zhou, J., Zou, A., Li, W., Yao, C., & Xie, S. (2010). DDSolver: An add-in program for modeling and comparison of drug dissolution profiles. *The AAPS Journal*, 12(3), 263–271. <https://doi.org/10.1208/s12248-010-9185-1>
- Zhao, Y., Khalid, N., Shu, G., Neves, M. A., Kobayashi, I., & Nakajima, M. (2019). Complex coacervates from gelatin and octenyl succinic anhydride modified kudzu starch: Insights of formulation and characterization. *Food Hydrocolloids*, 86, 70–77. <https://doi.org/10.1016/j.foodhyd.2018.01.040>
- Łupina, K., Kowalczyk, D., & Drożdowska, E. (2020). Polysaccharide/gelatin blend films as carriers of ascorbyl palmitate – a comparative study. *Food Chemistry*, 333, 127465. <https://doi.org/10.1016/j.foodchem.2020.127465>
- Łupina, K., Kowalczyk, D., Zięba, E., Kazimierzak, W., Mężyńska, M., Basiura-Cembala, M., & Ewa, A. (2019). Edible films made from blends of gelatin and polysaccharide-based emulsifiers - a comparative study. *Food Hydrocolloids*, 96, 555–567. <https://doi.org/10.1016/j.foodhyd.2019.05.053>